Advanced Composite Materials
Publication details, including instructions for authors and subscription information:
http://www.tandfonline.com/loi/tacm20

Influences of assembly parameters on the strength of bolted composite-metal joints under tensile loading

L. Liu [a] , J. Zhang [a] , K. Chen [a] & H. Wang [a]
[a] School of Aeronautics and Astronautics, Shanghai Jiao Tong University , 800 Dongchuan RD., Minhang District, Shanghai , 20040 , China
Published online: 09 Aug 2013.

To cite this article: L. Liu , J. Zhang , K. Chen & H. Wang (2013) Influences of assembly parameters on the strength of bolted composite-metal joints under tensile loading, Advanced Composite Materials, 22:5, 339-359, DOI: 10.1080/09243046.2013.824855

To link to this article: http://dx.doi.org/10.1080/09243046.2013.824855

Advanced Composite Materials, 2013
Vol. 22, No. 5, 339–359, http://dx.doi.org/10.1080/09243046.2013.824855

Influences of assembly parameters on the strength of bolted composite-metal joints under tensile loading

L. Liu*, J. Zhang, K. Chen and H. Wang

School of Aeronautics and Astronautics, Shanghai Jiao Tong University, 800 Dongchuan RD., Minhang District, Shanghai 20040, China

(*Received 23 March 2013; accepted 10 July 2013*)

Different assembly parameters, which include the bolt's clamping forces and bolt-hole interference fit conditions, can change the mechanical behaviours of the bolted composite joints under tensile loading. Three-dimensional finite element models with different bolt-hole fit conditions and bolts' preloads are constructed based on the contact relationships between the fasteners and the plates, the progressive failure features of composite materials and the elastic–plastic property of the titanium alloy. The models are used to study the effects of the assembly parameters after the modelling method is validated through comparing with test results. Through the analysis of the results, the conclusions can be drawn that: firstly, appropriate preload or interference fit can change the contact status and stress state around the fastener hole as the joints are under load and then increases the load capacity of the joints; secondly, too large preload or interference fit will cause joints to fail prematurely and decrease the load capacity consequently; thirdly, the effect of the bolt-hole fit conditions and the effect of the bolt's clamping forces impact each other, and these two parameters need to be considered together in order to obtain the optimized joint configurations.

Keywords: interference fit; clamping force; load capacity; composite; bolted joints

1. Introduction

Composite structures are used extensively in aircraft structures because of their excellent mechanical properties combined with low density, and fastener joining is a common method to assemble composite structures in aviation industry because of its reliability and its facility to assemble and disassemble.[1–3] However, joints tend to be the weakest part of the structure, since the enhanced stress concentration at the surrounding of the fastener hole and the weakness of the composite materials under out-of-plane loads often decreases the load capacity of the composite structures.[4,5] Comparing with metal structures, joining technology in composite laminates structures is a significant issue with 60–85% of failures occurring at the fastening joint.[6] Therefore, a major goal of composite bolted joint research is to determine the effect of various bolting parameters on the joint strength. A lot of parametric studies have already performed, and the conclusions have been drawn that the joint strength is influenced not only by joint geometric factors, material properties, coefficient of friction and bolt shapes, but also by the assembly parameters, such as the bolt's tightening torques and the fit conditions between the fastener shank and hole.[7]

*Corresponding author. Email: liulongquan76@sjtu.edu.cn

According to the experiences of metallic bolted joint, tightening torque can considerably prolong the fatigue life of the bolted plates as a result of introducing more compressive stresses around the plate hole,[8] and an optimal set of interference fit can enhance the fatigue life until crack re-initiation through changing the stress state around the fastener hole.[9] Fu-Kuo Chang et al. [10,11] have numerically and experimentally investigated the lateral constraining effect on bolted composite joints, and their research results show that the bolt clamping force can significantly reduce the notch tensile strength of filled-hole laminates composite laminates which are prone to fibre-matrix splitting and delamination; however, for bolted joints which fail in a net-tension mode, clamping improves the joint strength regardless of the ply orientation. Khashaba et al. [12] have studied the influence of the tightening torque on the mechanical properties of GFRE laminates experimentally and theoretically and find that in the range of the investigated tightening torques, the bearing strength of bolted joint increases with increasing tightening torque. Rosales-Iriarte et al. [13] have performed experimental researches about the influence of the tightening torque on the behaviours of composite joints, and high increase in bearing strength has been found when clamping forces are included in their research. Sen et al.[5] have performed experiments to determine the failure mode and bearing strength of mechanically fastened bolted joints in glass fibre-reinforced epoxy laminated composite plates, and the results show that failure modes and bearing strengths are considerable affected by the increasing of preloads as the preloads are between 0 and 6 Nm. However, the studies of Park [14] also show that though the lateral clamping pressure increases both the delamination and ultimate failure strengths of bolted joints in composite laminates, as the clamping pressure increases, the ultimate bearing strength shows a significant increase towards saturation, while the delamination bearing strength shows a progressive increase. The ultimate bearing strengths do not increase after the saturated bolt clamping pressure. Hence, it is desirable that the clamping torque of a bolted joint in a composite laminate should not exceed the saturated bolt clamping pressure.

Most of these studies have found that the bearing strength of bolted joints improves with the increase in tightening torque in a range for the specified joint configurations. However, the clamping force has both positive and negative sides of effects. The positive effect is that the lateral constraint produced by the tightening torque will suppress the local delamination to be onset and progress to some extent, and then, the load capacities of the joints will be increased. On the other hand, the negative effect is that inappropriate out-of-plane stresses can lead to a premature failure of the joint.[15,2] Therefore, there must be an appropriate tightening torque value for specific composite joint structures.

In clearance fit joints, the bolts can cause fretting damage during cyclic loading due to very small relative displacement of contacting surfaces of the bolt and plate.[16] And Chakherlou et al. [17,18] have investigated mechanical behaviours of bolted joints with different interference fit conditions using both experimental and numerical methods, and they have indicated that the interference fit joining can improve the fatigue life of metal structures. In the past, the general consensus was that interference fit joining was just suited to metallic materials and not suited to composite structures. The fit conditions between the fasteners and plates are normally 0.1 mm clearance fit in aircraft joints. [6,7] However, it has also been pointed out by formerly McDonnel Douglas Corp that some extent of interference fit joining improves the fatigue life of carbon epoxy composites.[19] Kiral [20] has constructed three-dimensional finite element models to examine the effects of the clearance and interference fit on the failure mode, failure load

and bearing strength of the pin-loaded joints subjected to traction forces, and he has concluded that the fit condition between the pin and the hole has an important influence on the failure load of mechanically fastened joints, and the failure loads are developed for all the studied joint configurations if interference fit is used. Kim et al. [21] have investigate the effect of interference fit on fatigue life of pin-loaded glass fibre-reinforced plastics (GFRP) composites, and they have found that, even with possible local damage on the joints, interference fit does not degrade the performance of the composite joints under quasi-static loading, especially when kept under 1 of interference fit. However, fatigue life is improved due to interference fit. Zhao et al. [22] have indicated that suitable interference can improve the fatigue life of composite/metal hybrid joints. Interference of 1.5–2.5% can all improve metal/composite joints fatigue life more than doubled. Wang et al. [23] have analysed the tangential stress at the hole edge of the cross-area in composite interference fit joints using ANSYS software, and the distributions of dangerous fatigue points on each plate are obtained. Whereas, too large interference between the bolt and hole will introduce interlaminar shearing stress and cause delamination around the hole boundary and then will decrease the joint strength. [24,25] Therefore, there must be an appropriate interference value for specific composite joint structures.

From all the aforementioned descriptions, it can be seen that the effects of either the bolt-hole fit condition or the clamping force have been separately investigated a lot in the past. However, seldom of these studies involves into the optimized values of both the fastener's preload and the bolt-hole fit; furthermore, both these two parameters may impact each other on their effects because they both influence the mechanical behaviour of the bolt joints through changing the stress state around the fastener hole. Thus, both of these two assembly parameters need to be studied together to optimize the joint structures. Consequently, the main objective of this study is to investigate the combined effect of interference fit and clamping force on the load capacity of the single-lap composite joints. To aim this, in the following text of this paper, an experimental validated three-dimensional finite element modelling method is introduced to simulate the mechanical behaviours of the joints with different combinations of clamping forces and bolt-hole fits, and the results of the joints with different assembly parameters are compared and analysed.

2. Problem statements

Woven fabric and unidirectional tape lamina are sometimes used together to form hybrid composite material in order to take full advantages of the high resistance to impact performances of woven fabric and the high unidirectional mechanical performances of unidirectional lamina. In addition to that, the composite material and titanium alloy are usually used together to take full advantages of their properties, such as low density of the composite materials and high bearing capacities of the metallic materials. In such cases, bolt joining techniques are usually required to join the composite and metallic materials together. In current study, an aft pressure bulkhead (spherical dome) is made of such kind of hybrid composite materials, and this composite cabin connects to the titanium alloy frame of the aft fuselage via two rows of hi-lock fasteners along the circumferential direction of the airframe.

Three different kinds of composite-to-titanium two-bolt single-lap joint specimens are used to represent the configurations of the bulkhead-to-fuselage joints with different bolt-hole fit conditions in order to study the mechanical performances of the joint

structure. Except for the fasteners and holes, all of the other geometries and dimensions of the three different joints are all the same, which are shown in Figure 1. The locations and dimensions tolerances in Figure 1 conform to the general tolerance requirements for composite products HB 7741-2004.

The composite plate and titanium plate are joined together by HST fasteners, and the differences between the three kinds of joints are detailed in Table 1.

Thus, the fit conditions between the fastener shanks and holes of the joint-1 and joint-3 are neat fit and that of the joint-2 is 1.5% interference fit. Unlike usually used bolt and nut assemblies, the clamping forces of the hi-shear fastener are not adjustable, and a specified hi-shear fastener has a constant clamping force. And the clamping force is depended on the geometry characters of the fastener assembly, thus the same fastener will have the same clamping force, and the clamping force is dependent on the force (moment) of breaking the collar. The material of the HI-LITE pin is annealed titanium alloy, Ti6Al4 V, manufactured per AMS 4967[26], and its tensile strength is 1103 MPa (160000 psi). The elastic–plastic mechanical properties of the Ti6Al4 V can also refer to Mil-Handbook 5.[28] The clamping force introduced by breaking the hi-lock collar is about 20% strength of the related fastener shank according to the preload test results of Huang and Wang [29]; therefore, both the clamping forces of the joint-1 and joint-2 are 4 kN, and the clamping force of the joint-3 is 3.2 kN.

The material of the composite plate is a hybrid material manufactured from unidirectional tape lamina (CYCOM 977-2A-37%-3KHTA-5HS-280-1200 [30]) and twill woven carbon fabric composite (CYCOM 977-2-35%-12KHTS-134-300 [31]) with stacking sequence being $[(\pm45)/0/\pm18/\pm36/+54/(0/90)/-54/\pm72/90]_s$. In the stacking sequence, the unidirectional tape lamina is represented as angles, such as 0, ±18 and 90. The woven fabric lamina is represented as '(angles)', such as (±45) and (0/90). The material system of the laminate coincides with the geometry coordinate system of the specimen, which means the '1', '2' and '3' directions of the unidirectional tape lamina with 0 degree and the '*L*', '*T*' and '*Z*' directions of the woven fabric with 0 degree are coincident with the '*X*', '*Y*', and '*Z*' directions of the coordinate system shown in Figure 1, respectively. The '1', '2' and '3' directions are the longitudinal, transverse and thickness directions of the unidirectional tape lamina, and '*L*', '*T*' and '*Z*' directions are the warp, weft and thickness directions of the woven fabric lamina. The nominal cured ply thicknesses of the unidirectional tape and woven fabric are 0.131 and 0.295 mm, respectively, and the mechanical properties of the two different laminas are shown in Tables 2 and 3, respectively. Because the thickness properties of the composite are very difficult to obtain, it is customarily assumed that the matrix properties apply in the thickness direction.[32] Therefore, it can be said $E_{22} = E_{33}$, $V_{12} = V_{13}$ and $v_{21} = v_{31}$ apply for the unidirectional lamina.

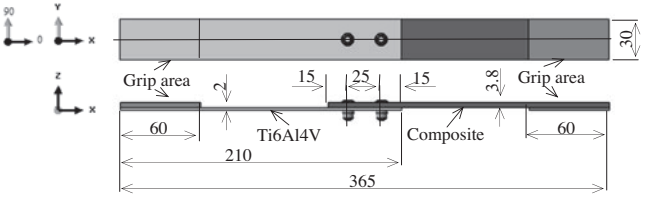

Figure 1. Specimen geometry dimensions (all dimensions in mm).

Table 1. The configuration of the test specimens.

Joint configuration	Fastener type	Shank diameter (mm)	Hole diameter (mm)
Joint-1	HST10AP6 [27] + HST1094-6 [28]	4.8 ± 0.013	$4.8_{0}^{+0.01}$
Joint-2	HST10AP6 + HST1094-6	4.8 ± 0.013	$4.8_{-0.1}^{-0.04}$
Joint-3	HST10AP5 [27] + HST1094-5 [28]	4.14 ± 0.013	$4.14_{0}^{+0.01}$

Table 2. Mechanical properties of the unidirectional tape lamina [30].

Elastic property	E_{11} (GPa)	E_{22} (GPa)	E_{33} (GPa)	G_{12} (GPa)	G_{13} (GPa)	G_{23} (GPa)	υ_{12}	υ_{13}	υ_{23}
Value	131.85	9.14	9.1	5.13	5.13	3.672	0.3	0.3	0.48
Strength property	S_{11}^{T} (MPa)	S_{11}^{C} (MPa)	S_{22}^{T} (MPa)	S_{22}^{C} (MPa)	S_{33}^{T} (MPa)	S_{33}^{C} (MPa)	S_{12} (MPa)	S_{13} (MPa)	S_{23} (MPa)
Value	2104	1407	81.56	360.5	81.4	488.4	135.5	45.3	135.5

Table 3. Mechanical properties of the woven fabric lamina [31].

Elastic property	E_{L} (GPa)	E_{T} (GPa)	E_{Z} (GPa)	G_{LT} (GPa)	G_{TZ} (GPa)	G_{LZ} (GPa)	υ_{LT}	υ_{LZ}	υ_{TZ}
Value	66.16	61.04	20.24	6.54	8.76	8.76	0.04	0.03	0.03
Strength Property	$S_{\mathrm{L}}^{\mathrm{T}}$ (MPa)	$S_{\mathrm{L}}^{\mathrm{C}}$ (MPa)	$S_{\mathrm{T}}^{\mathrm{T}}$ (MPa)	$S_{\mathrm{T}}^{\mathrm{C}}$ (MPa)	$S_{\mathrm{Z}}^{\mathrm{T}}$ (MPa)	$S_{\mathrm{Z}}^{\mathrm{C}}$ (MPa)	S_{LT} (MPa)	S_{TZ} (MPa)	S_{LZ} (MPa)
Value	895.5	922.6	872.6	885.7	80.7	480.1	119	80.7	80.7

3. Finite element simulation

3.1. Meshes and boundary conditions

The three joints described in Table 1 are modelled using ABAQUS software.[33] The modelling methods of the three joints are the same except the detail geometries of the fasteners and holes. The finite element model of the joint-1, which is shown in Figure 2, is treated as an example to describe the modelling process. Since the behaviour of balanced symmetric laminate is studied and the geometry of the problem is symmetric with respect to the XZ plane, and considering that the composite plate is comparatively thick, only half of the joint is modelled. Because the effective lengths of the plates are 150 mm, both the composite and titanium plates are modelled to be 150 mm long and 15 mm wide.

To avoid the shear locking problem and to decrease the computing time, the reduced linear eight-node isoparametric three-dimensional solid elements, C3D8R, are utilized to model the fasteners, the metallic plate and each ply of the laminate plate (except for the elements surrounding the fastener hole). The area covered by the fastener head/nut is refined meshed (10 elements along the radius direction) as full integration incompatible linear eight-node isoparametric three-dimensional solid elements, C3D8I, to ensure the accurate contact results and capture the stress gradients. Per ply is modelled as on element in thickness direction, which can provide a reasonable approximation of the

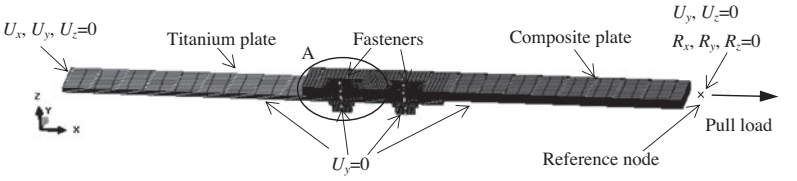

a) Meshes and boundary conditions

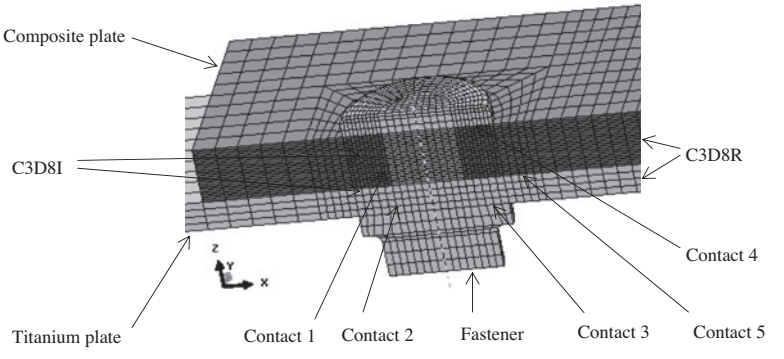

b) Detail View A

Figure 2. Finite element model.

through-the-thickness stresses. There are 40 elements around the circumferential direction of the fastener hole; thus, the aspect ratio of the elements around the fastener hole is about 2.5. The clamping force introduced by the tightening torque was applied through 'Bolt load' function in Abaqus CAE, and it is set to be 2 kN for half of the intersection area of the fastener shank in joint-1 and joint-2 and 1.6 kN in joint-3.

The boundary conditions of the three different kinds of specimen finite element model are the same, which are shown in Figure 2. The symmetric surfaces of the two joint plates and fasteners are constrained in translational direction U_y and rotational directions R_x and R_z. The left end of titanium plate is held fixed in all three translational directions (U_x, U_y and U_z). The right end of the laminate plate has 'tie' relationship with a reference node. Thus, the motion of the right side surface is governed by the motions of the reference node, which is held fixed in two translational directions (U_y and U_z) and all three rotational directions (R_x, R_y and R_z), while a pull load is applied in U_x direction.

3.2. Contact relationships

The contact relationships in the joints are defined via the interactive module of Abaqus software. Because the nut and fastener shank are engaged together, they are modelled as one part to decrease the contact surfaces and shorten the processing time in computer. There are totally nine contact pairs in the two-bolt composite-to-titanium joint. Four of them are located between the fasteners shanks and holes (including two contact pairs for each fastener), four of them are between fastener heads/nuts and the outer surfaces of the two plates (including two contact pairs for each fastener), and one of them is between the faying surface of two plates (including one contact pair).

The contact pairs around one of the fasteners are shown in Figure 2(b). Finite sliding formulation is used to model all the contact relationships. The bolt-hole fit conditions can be changed through setting the 'Interference fit' values of the four contact pairs between the fastener shanks and holes. The frictional coefficient between titanium materials is set to be 0.4 referring to Ref. [35] and that between the titanium material and composite material is set to be 0.1 referring to Refs. [2,34].

3.3. Material models

The failure modes of the unidirectional tape lamina include fibre tensile/compression failure, matrix tensile/compression failure and delamination, and the failure modes of the trill woven composite include warp tensile/compression failure, weft tensile/compression failure and delamination.

Generally, progressive failure analysis consists of two major steps.[35] The first step is to choose appropriate failure criteria to justify which kind of failure mode occurs prior to others. For failure prediction, the maximum stress criterion, the maximum strain criterion, Hoffman criterion, Tsai–Wu criterion and Hashin criterion are employed in many failure predictions for composite materials. The laminates modelled in the composite plate adopted Hashin and Ye failure criteria.[36,37] The failure criteria of unidirectional lamina and woven fabric are shown in Tables 4 and 5, respectively.where (i, j = 1, 2, 3) are the scalar components of the stress tensor, and S_{ij} (i, j = 1, 2, 3) are the material strengths (the '1', '2' and '3' directions are the longitudinal, transverse and thickness directions of the unidirectional tape lamina, respectively); the superscripts T and C denote tension and compression, respectively.

The second step is to choose a suitable material degradation rule for reduction in stiffness of the composite material after a certain type of failure has occurred. The commonly used degradation methods are the total discount method, the limit discount method and the residual property method. The limit discount method of the unidirectional lamina in this research is referred to the degradation rules of Tan [38] and that of the woven fabric is referred to Zhao [39], which are shown in Tables 6 and 7, respectively.

As for composite materials, the failure criterion and the degradation rule are implemented using ABAQUS user subroutine USDFLD, and the state variables depend on the failure criterion for each damage mechanism. These state variables are passed in the beginning of iteration and, if damage does not occurred previously at an element

Table 4. Failure criteria of unidirectional lamina.

Failure mode	Failure criterion
Fiber tensile failure ($\sigma_{11} \geqslant 0$)	$\left(\frac{\sigma_{11}}{S_{11}^T}\right)^2+\left(\frac{\sigma_{12}}{S_{12}}\right)^2+\left(\frac{\sigma_{13}}{S_{13}}\right)^2 \geqslant 1$
Fiber compressive failure ($\sigma_{11}<0$)	$\left(\frac{\sigma_{11}}{S_{11}^C}\right)^2 \geqslant 1$
Matrix tensile failure ($\sigma_{22}+\sigma_{33} \geqslant 0$)	$\left(\frac{\sigma_{22}+\sigma_{33}}{S_{22}^T}\right)^2+\frac{\sigma_{23}^2-\sigma_{22}\sigma_{33}}{S_{23}^2}+\left(\frac{\sigma_{12}}{S_{12}}\right)^2+\left(\frac{\sigma_{13}}{S_{13}}\right)^2 \geqslant 1$
Matrix compressive failure ($\sigma_{22}+\sigma_{33}<0$)	$\frac{1}{S_{22}^C}\left[\left(\frac{S_{22}^C}{2S_{23}}\right)^2-1\right](\sigma_{22}+\sigma_{33})+\left(\frac{\sigma_{22}+\sigma_{33}}{2S_{23}}\right)^2+\frac{1}{S_{23}^2}(\sigma_{23}^2-\sigma_{22}\sigma_{33})+\left(\frac{\sigma_{12}}{S_{12}}\right)^2+\left(\frac{\sigma_{13}}{S_{13}}\right)^2 \geqslant 1$
Delamination	$\left(\frac{\sigma_{33}}{S_{33}^T}\right)^2+\left(\frac{\sigma_{13}}{S_{13}}\right)^2+\left(\frac{\sigma_{23}}{S_{23}}\right)^2 \geqslant 1, \sigma_{33} \geqslant 0$ $\left(\frac{\sigma_{33}}{S_{33}^C}\right)^2+\left(\frac{\sigma_{13}}{S_{13}}\right)^2+\left(\frac{\sigma_{23}}{S_{23}}\right)^2 \geqslant 1, \sigma_{33}<0$

Table 5. Failure criteria of woven fabric composite.

Failure mode	Failure criterion
Warp tensile failure ($\sigma_{11} \geqslant 0$)	$\left(\frac{\sigma_{11}}{S_{\mathrm{L}}^{\mathrm{T}}}\right)^2+\left(\frac{\sigma_{12}}{S_{\mathrm{LT}}}\right)^2+\left(\frac{\sigma_{13}}{S_{\mathrm{LZ}}}\right)^2 \geqslant 1$
Warp compressive failure ($\sigma_{11}<0$)	$\left(\frac{\sigma_{11}}{S_{\mathrm{L}}^{\mathrm{C}}}\right)^2 \geqslant 1$
Weft tensile failure ($\sigma_{22} \geqslant 0$)	$\left(\frac{\sigma_{11}}{S_{\mathrm{T}}^{\mathrm{T}}}\right)^2+\left(\frac{\sigma_{12}}{S_{\mathrm{LT}}}\right)^2+\left(\frac{\sigma_{23}}{S_{\mathrm{TZ}}}\right)^2 \geqslant 1$
Weft compressive failure ($\sigma_{22}<0$)	$\left(\frac{\sigma_{22}}{S_{\mathrm{T}}^{\mathrm{C}}}\right)^2 \geqslant 1$
Delamination	$\left(\frac{\sigma_{33}}{S_{\mathrm{Z}}^{\mathrm{T}}}\right)^2+\left(\frac{\sigma_{13}}{S_{\mathrm{LZ}}}\right)^2+\left(\frac{\sigma_{23}}{S_{\mathrm{TZ}}}\right)^2 \geqslant 1, \sigma_{33} \geqslant 0$
	$\left(\frac{\sigma_{33}}{S_{\mathrm{Z}}^{\mathrm{C}}}\right)^2+\left(\frac{\sigma_{13}}{S_{\mathrm{LZ}}}\right)^2+\left(\frac{\sigma_{23}}{S_{\mathrm{TZ}}}\right)^2 \geqslant 1, \sigma_{33}<0$

Table 6. Degradation rules of the unidirectional tape lamina.

Failure mode	E_{11} (MPa)	E_{22} (MPa)	E_{33} (MPa)	υ_{12}	υ_{13}	υ_{23}	G_{12} (MPa)	G_{13} (MPa)	G_{23} (MPa)
No failure	131,850	9140	9140	0.3	0.3	0.42	5130	5130	3672
Fiber failure	26,370	9140	9140	0.06	0.06	0.42	1026	1026	3672
Matrix failure	131,850	1828	9140	0.06	0.3	0.084	1026	5130	734.4
Delamination	131,850	9140	1828	0.3	0.06	0.084	5130	1026	734.4

Table 7. Degradation rules of the weave tape lamina.

Failure mode	E_{L} (MPa)	E_{T} (MPa)	E_{z} (MPa)	υ_{LT}	υ_{LZ}	υ_{TZ}	G_{LT} (MPa)	G_{LZ} (MPa)	G_{TZ} (MPa)
No failure	66,160	61,040	20,000	0.04	0.3	0.3	16,500	11,000	11,000
Warp failure	13,232	61,040	20,000	0.008	0.06	0.3	3300	2200	11,000
Weft failure	66,160	12,208	20,000	0.008	0.3	0.06	3300	11,000	2200
Delamination	66,160	61,040	4000	0.04	0.06	0.06	16,500	2200	2200

integration point, that element was checked for damages, and the state variables are updated. These solution-dependent state variables are then used to create an array of field variables that define the material properties for the next iteration.

4. Model validation

To validate the three-dimensional finite element modelling method for the composite joint, simulation results are compared with the experimental results, and two characteristics, load-displacement curves and bearing strain-load curves, are utilized as the criteria.

Quasi-static tests of the specimens were conducted using a MTS Landmark electron-hydraulic servo-controlled material testing machine as shown in Figure 3. The Figure 3(a) illustrates the test set-up method, and the Figure 3(b) illustrates the strain measurement method. The joint specimen was clamped by the two heads of the testing machine, and tensile load was applied to the specimen through fixing the stationary head and moving up the moveable head. One YYJ-1040 electronic extensometer, whose

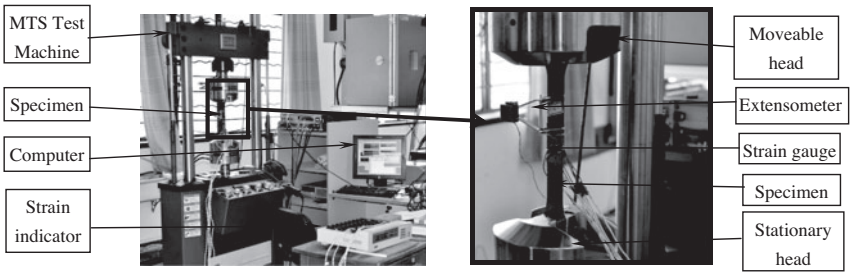

(a) Specimen installation method

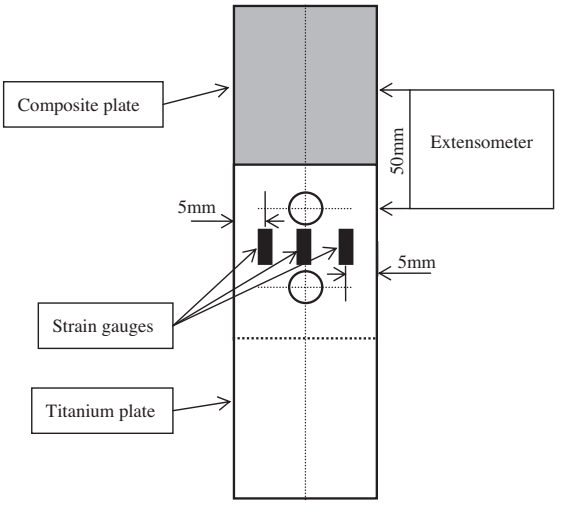

(b) Strain measurement method

Figure 3. Test setup.

gauge length is 50 mm and accuracy is 0.036%, was used to measure the bearing deformation of the fastener hole. The test set-up method and the bearing measurement method are based on the composite bearing response and bearing/bypass interaction response test standards of American Society for Testing and Materials, ASTM D 5961/D5961M-08 [40] and ASTM D 7248/D7248M-08.[41] In order to avoid the bending effect, three BX120-3AA strain gauges, whose accuracy is 1%, were used to centre aligned the specimens in accordance with the test standard of American Society for Testing and Materials, ASTM D 3039-08.[42] Two strain gauges are pasted on the outer surface metallic plate, they locate in the middle of the two fasteners and the distances between the centre lines of the strain gauges and the edge of the joint are 5 mm. The other strain gauge is in the middle of the two strain gauges mentioned above and pasted on the outer surface of the composite plate. The quasi-static tensile tests were performed in displacement control mode with the constant speed being 1 mm/min, which kept proceeding until the joint cannot take any further load. The circumstance temperature was kept being 23±5 °C, and the relative humidity was kept being 5±5% during test.

The comparisons of the load-displacement curves between the test results and the simulation results are shown in Figure 4. The load-displacement curves in both Figure 4

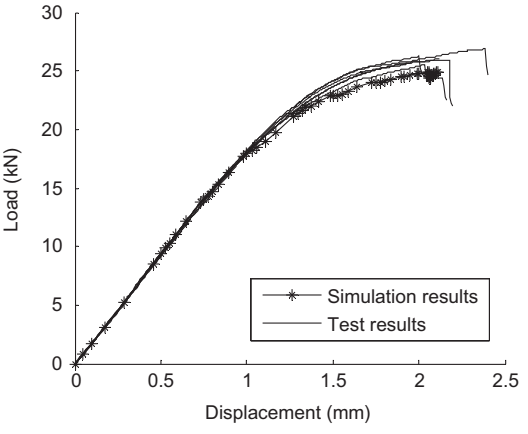

(a) Joint-1

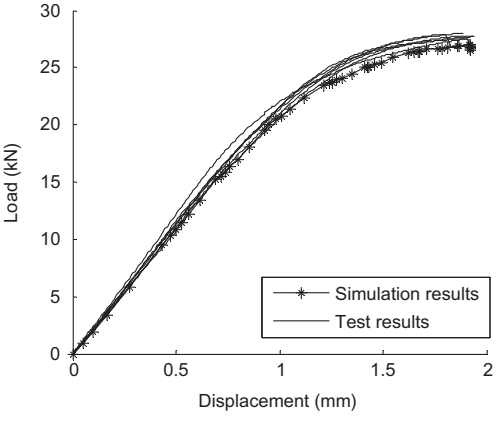

(b) Joint-2

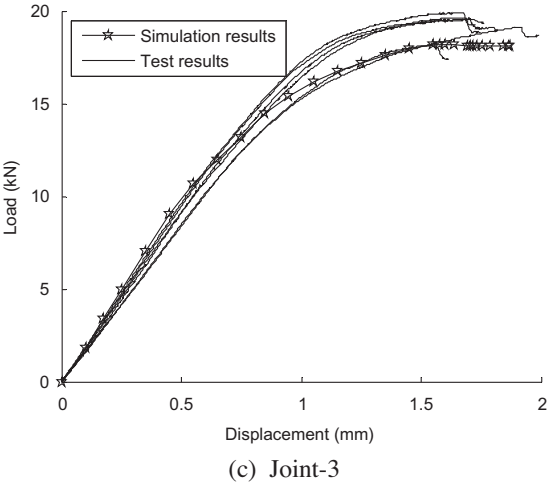

(c) Joint-3

Figure 4. Comparisons of load-displacement curves between test and simulation results.

(a–c) are linear in the beginning process of the loading, following that, the slopes of the curves keep declining, which means that the stiffness values of the joints are decreasing and certain kinds of failures have taken place. Finally, the loads reach their summits, and the stiffness of the joints decreases to zero. The maximum load values of the joint-2 are bigger than the joint-1; however, the maximum displacement of the joint-2 is smaller than that of the joint-1. Both the maximum load and maximum displacement joint-3 are lower than that of joint-1.

It can also be seen from Figure 4(a) that the mean value of the maximum test loads is 26,158 N and the maximum load of the simulation result of joint-1 is 24,914 N. The difference between the simulation results and the test results of the joint-1 is about 4.7%. From Figure 4(b), it can be seen that the mean value of the maximum test loads is 27,918 N and the maximum load of the simulation result of joint-2 is 26,844 N. The difference between the simulation results and the test results of the joint-2 is about 4.0%. From Figure 4(c), it can be seen that the mean value of the maximum test loads is 19,308 N and the maximum load of the simulation result of joint-3 is 18,097 N. The difference between the simulation results and the test results of the joint-3 is about 6.3%. Therefore, the simulation results agree well with the test results in regard to the load–displacement relationships.

According to ASTM D 5961/D5961M-08 [37], the bearing strains of the single-lap joints can be demonstrated as:

$$\varepsilon^{\mathrm{br}} = \frac{\delta}{2 \times D} \tag{1}$$

where the D represents the diameter of the fastener hole and δ represents the deformation obtained by the extensometer.

The bearing strains of three specimens in each batch of specimens are measured, and the comparison of the bearing strain-load curves between the test results and simulation results is shown in Figure 5. Similar to what is shown in Figure 4, the bearing strain–load relationships of the simulation results agree with that of the test results quite well. It is worth to mention that the bolted joints can normally be seen fail when the bearing strain reaches 4 percentage.

Therefore, through the comparison with the test results on both the load-displacement curves and the bearing strain-load curves of the joints, the simulation results are found to be consistent and in agreement with the experimental test results, and these validate the modelling method of the composite-to-titanium single-lap joint proposed in this paper.

5. Simulation conditions

For the intentional interference fitting, the fastener shank and the hole are not matched exactly, and the misfit is defined by a parameter λ which relates the hole radius a and the fastener shank radius $a_{//}$ [43]:

$$a_{//} = a(1 + \lambda) \tag{2}$$

The joints with different fit conditions (λ being 0, 0.5, 1, 1.5, 2, 2.5 and 3%) and clamping forces (P being 0, 2000, 4000 and 6000 N) are simulated via the experimental validated numerical modelling method.

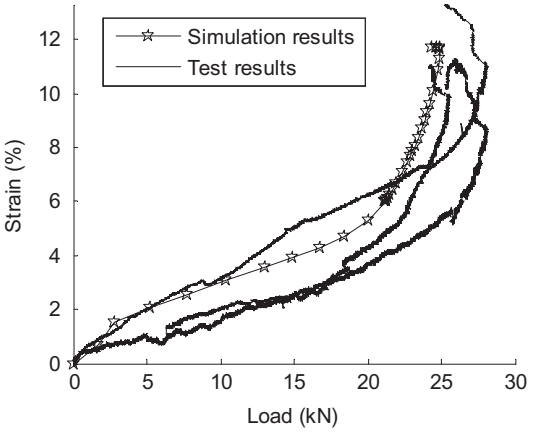

(a) Joint-1

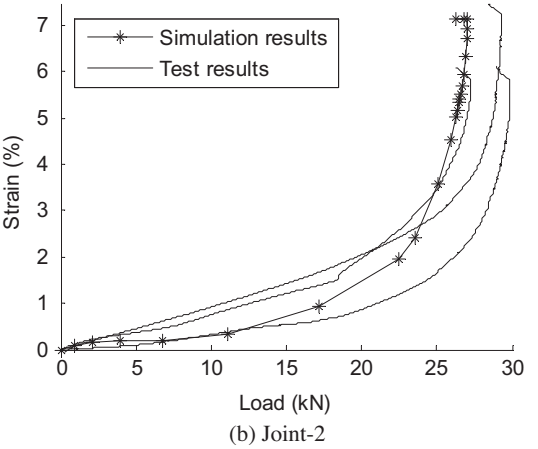

(b) Joint-2

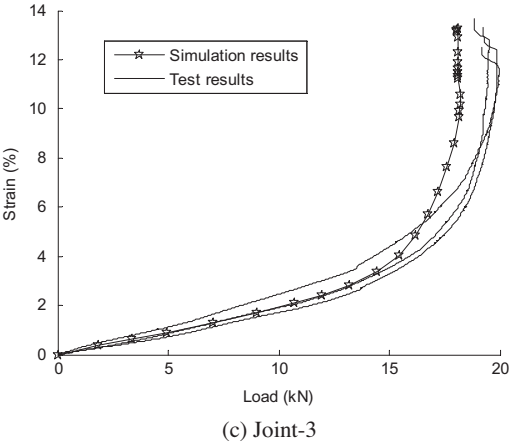

(c) Joint-3

Figure 5. Comparisons of strain-load curves between test and simulation results.

6. Results and discussions

6.1. The influence of bolt-hole fit conditions

The load-displacement curves of the joints with the same clamping forces (4 kN) but different fastener-hole fit conditions are shown in Figure 6, from which it can be seen that the load capacities of the joints increase with the increase in bolt-hole fit conditions when the interference fit values are smaller than 1.5%, and the load capacity decreases with the increase in bolt-hole conditions when the interference fit values are bigger than 1.5%. Therefore, the effect of bolt-hole fit conditions on the load capacities of the joints changes from positive mode into negative mode with the increase in the interference fit values. For the specific joint configuration described in this study, the joint with 1.5% interference fit has the highest load capacity.

Since the load capacity of the fibre-reinforced composite materials is mainly depended on the strength and failure conditions of the lamina in fibre direction (longitude direction), the fibre failure states around the fastener holes of the joints with different fastener-hole interference fit values (0, 1.5 and 3%) are compared as shown in Figure 7. Figure 7(a) shows the fibre failure condition the joint with neat fit under 0 N load, and Figure 7(d) shows the fibre failure condition of joint with neat fit under 20 N load. Figure 7(b) and (e) shows the fibre failure conditions of the joint with fastener-hole fit value being 1.5%. Figure 7(c) and (f) shows the fibre failure conditions of the joint with fastener-hole fit value being 3%.

From the comparisons among Figure 7(a–c), it can be seen that, before the tensile loads are applied to the joints, the fibre failure area around the fastener hole increases with the increase in the bolt-hole interference fit conditions. Whereas, from the comparisons among the Figure 7(d–f), it can be seen that, as the joints are loaded to 20 kN, the fibre failure area of the joint with 1.5% interference fit is the smallest among the three different joints. This partially explains the reason that the joint with 1.5% interference fit has higher load capacity than the joints with neat fit 3% interference fit.

Figure 8 illustrates the corresponding contact stress distributions surrounding the hole of the joints under the same condition as shown in the Figure 7. From the comparisons among Figure 8 (a–c), it can be seen that, before the joints are loaded, there is no contact stress distributing around the fastener hole of the joints with neat fit, but there are a certain extent of contact stress distributing around the fastener hole of the joints with 1.5 and 3% interference fits, and the peak contact stress of the joints

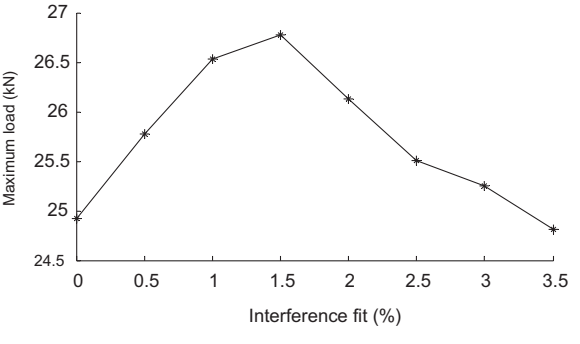

Figure 6. Load capacity of joints with different interference fit conditions.

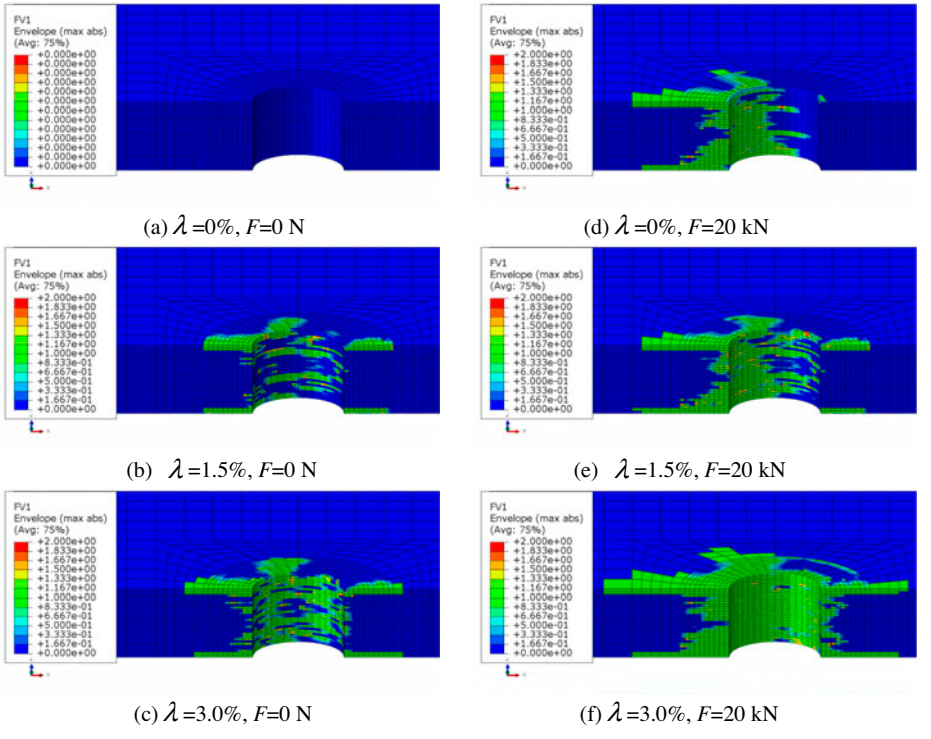

Figure 7. Fiber failure of the joints with different interference fits.

with 3% is 1795 MPa, which is the highest among the peak contact stress of the three different joints. From the comparisons among the Figure 8(d–f), it can be seen that, after the joints are loaded to 20 kN, the contact areas of the joints with 1.5 and 3% interference fit are bigger than that of the joint with neat fit, and the peak contact stress of the joint with 1.5% is about 2281 MPa, which is the lowest among the peak contact stress of the three different joints. This explains the reason that the fibre failure area of joint with 1.5% interference fit is the smallest among those of the three different joints.

Synthetically considering the contact stress and fibre failure surround the fastener hole shown in Figures 7 and 8, the conclusions can be drawn that the contact stress distribution surrounding the hole is very uneven for the joints with neat fit under tensile loading, which causes large range of fibre damage on the bearing side and premature failure of the structure; for the joints with 3% interference fit, the contact stress distribution is relatively uniform before and after loading. Exaggerated initial stress produced since the interference fit is too large, which will generate premature failure and reduce the carrying capability of the structure in turn; the 1.5% interference fit value suits the composite joint structures the best by producing some initial stress before loading and relatively uniform contact stress between bolt and plates after loading, which maximizes the strength of the joints. Therefore, the effect of the bolt-hole interference fit condition on the joint strength will change from positive into negative mode with the increase in the interference fit values, and for the joints with 4 kN preload described in this section, the 1.5% interference fit can provide the maximum load carrying capacity.

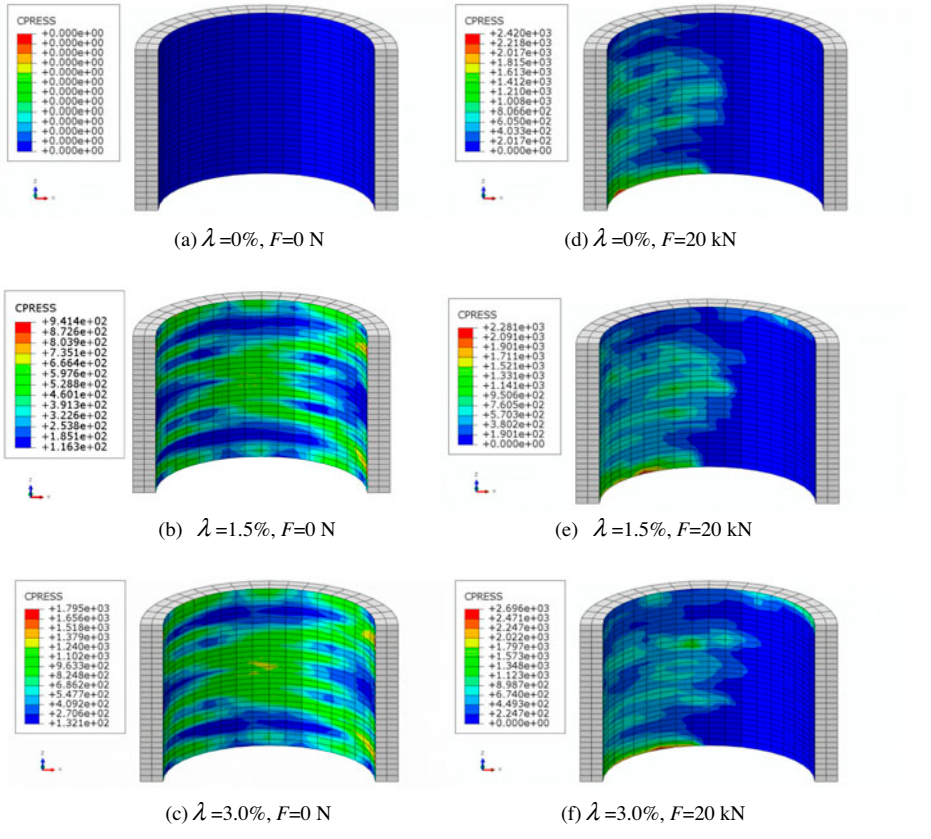

(a) λ =0%, F=0 N (d) λ =0%, F=20 kN

(b) λ =1.5%, F=0 N (e) λ =1.5%, F=20 kN

(c) λ =3.0%, F=0 N (f) λ =3.0%, F=20 kN

Figure 8. Contact stress distributions of the joints with different interference fit conditions.

6.2. The effect of clamping force

The maximum loads of the joints with the same interference fit value (1.5%) but different clamping forces are shown in Figure 9. From the Figure 9, it can be seen that the load capacities of the joints increase with the increase in the clamping forces when the clamping forces are smaller than 4 kN. However, the load capacities decrease with the increase in clamping forces when the clamping forces are bigger than 4 kN. Therefore, the effect of clamping force on the load capacities of the joints changes from positive mode into negative mode with the increase in clamping forces. For the specific joint configuration described in this study, the joint with the fasteners' clamping forces being 4 kN achieves the maximum load capacity.

The fibre damage failure conditions of the joints with three clamping force (P are 0, 4 and 6 kN, respectively) before and after loading are shown in Figure 10. Figure 10(a) illustrates the fibre failure condition the joint with fasteners' clamping force being 0 kN and tensile load being 0 kN, and Figure 10(d) illustrates the fibre failure condition of joint with fasteners' clamping force being 0 kN and tensile load being 20 kN. Figure 10 (b) and (e) illustrates the fibre failure conditions of the joint with fasteners' clamping force being 4 kN. Figure 10(c) and (f) illustrates the fibre failure conditions of the joint with fasteners' clamping force being 6 kN.

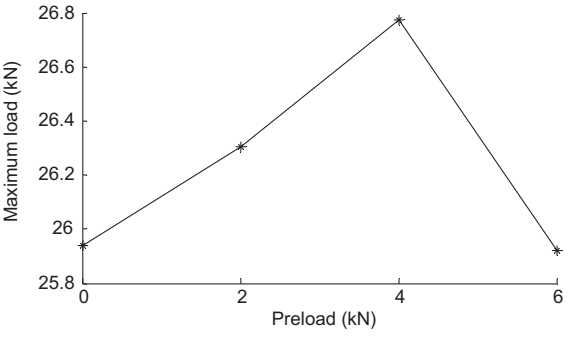

Figure 9. Load capacity of joints with different clamping forces.

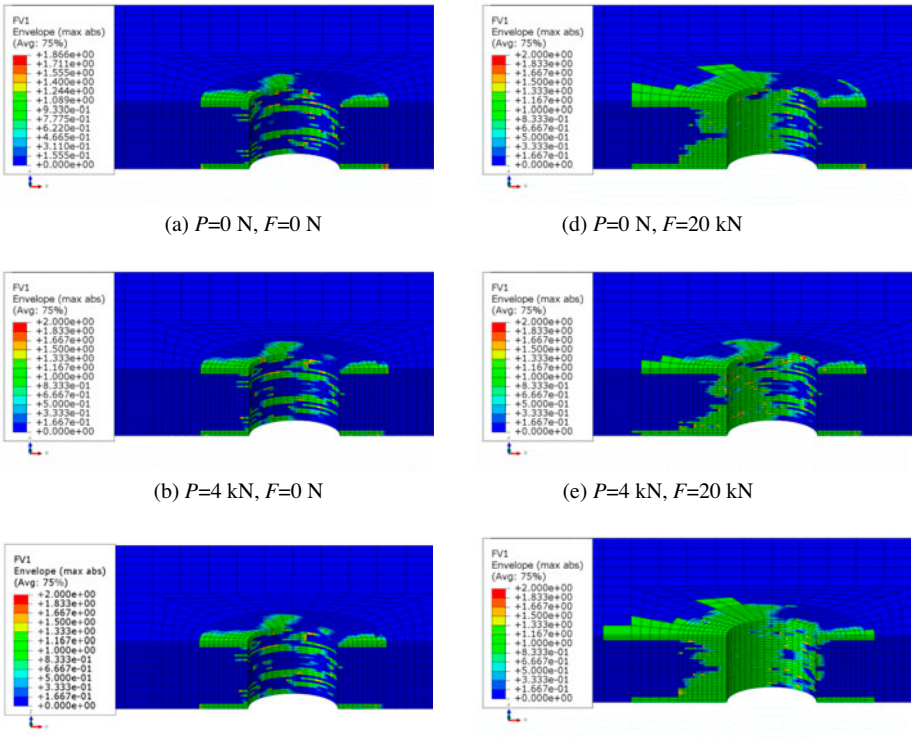

(a) P=0 N, F=0 N (d) P=0 N, F=20 kN

(b) P=4 kN, F=0 N (e) P=4 kN, F=20 kN

(c) P=6 kN, F=0 N (f) P=6 kN, F=20 kN

Figure 10. Fiber failure of the joints with 1.5% interference fit and different preloads.

From the comparisons among Figure 10(a–c), it can be seen that, before the tensile loads are applied to the joints, there are some extent of fibre failure surrounding the fastener hole for all joints with three different clamping forces, and the fibre failure area increases with the increase in the clamping forces. This is because the delamination area will increase with the increase in the clamping forces, and then, the stress will redistributed in the surrounding area of the fastener hole, and finally, this will induce some more fibre failure. Whereas, from the comparisons among the Figure 10(d–f), it can be

seen that, as the joints are loaded to 20 kN, the fibre failure area of the joint with 0 kN clamping force as shown in Figure 10(d) will be larger than that of the joint with 4 kN clamping force as shown in Figure 10(e), which indicates that certain clamping force may have some initial impact on fibre damage, but it can prevent the damage evolution at the loading process, which is beneficial to joints strength; the fibre failure area of the joint with 6 kN clamping force as shown in Figure 10(f) is also larger than that of the joint with 4 kN clamping force as shown in Figure 10(e), this is because 6 kN clamping force is overlarge for the composite structure, and the too large clamping force aggravates the spread of fibre damage instead of preventing it. Therefore, the joint with 4 kN clamping force has higher load capacity comparing with the joints with clamping forces being 0 and 6 kN.

Figure 11 illustrates the corresponding contact stress distributions surrounding the hole of the joints under the same condition as shown in the Figure 10. From the comparisons among Figure 11(a–c), it can be seen that, before the joints are loaded, the contact stress distribution and values are almost the same for the three different joints, and the contact stresses of the joints with preloads are a little higher than the contact stresses of the joints without preloads. From the comparisons among the Figure 11(d–f), it can be seen that, after the joints are loaded to 20 kN, the difference among the contact stresses of the joints with different preloads is larger, and the peak contact stress of joint with 4 kN preload is 2281 MPa, which is the lowest among the that of the three

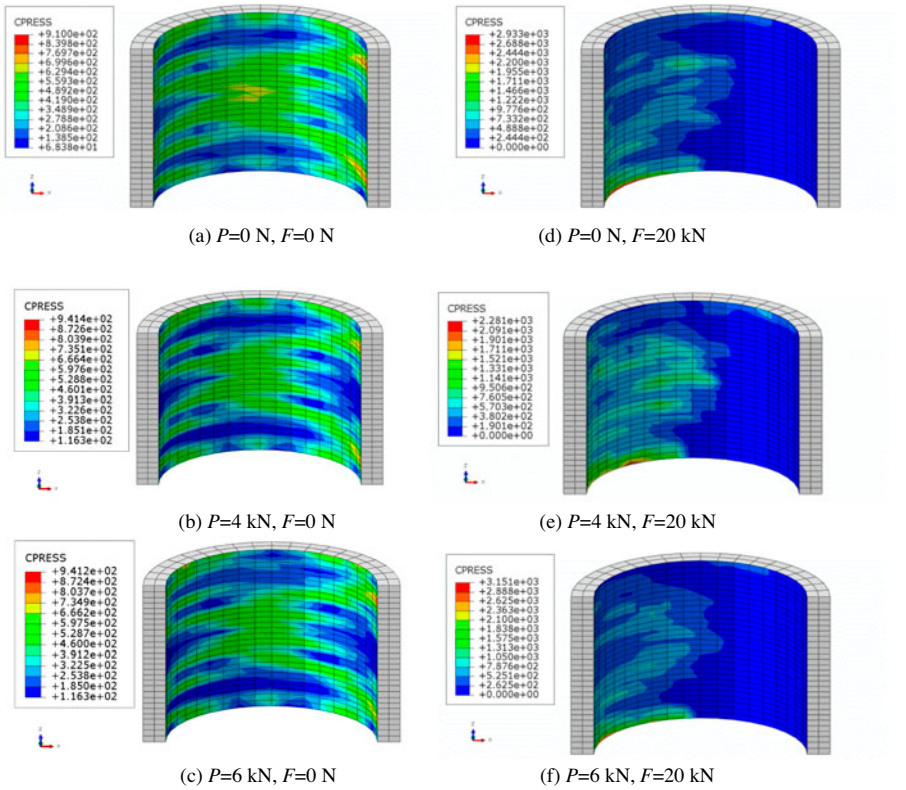

(a) P=0 N, F=0 N (d) P=0 N, F=20 kN

(b) P=4 kN, F=0 N (e) P=4 kN, F=20 kN

(c) P=6 kN, F=0 N (f) P=6 kN, F=20 kN

Figure 11. Contact stress distributions of the joints with 1.5% interference fit and different preloads.

different kinds of joints. This explains the reason that the fibre failure area of joint with 4 kN preload is the smallest among those of the three different joints.

Synthetically considering the contact stress and fibre failure surrounding the fastener hole shown in Figures 10 and 11, the conclusions can be drawn that the effect of the fasteners' preload on the joint strength changes from positive into negative mode with the increase in the preload values, and the 4 kN preload can provide the maximum load carrying capacity for the joints with 1.5% interference fit described in this section.

6.3. The combined effect

The maximum loads of the joints with different bolt-hole interference fit conditions and fastener's clamping forces are shown in Figure 12. From the Figure 12, it can be seen that, when the clamping force is lower than 4 kN, the joint with 1.5% interference fit value has the highest load capacity. However, when the clamping force is 6 kN, the load capacity of the joint with 1.5% interference fit is not the highest anymore, and the joint with 1% interference fit value has higher load capacity than the joint with 1.5% inference fit value. On the other hand, when the bolt-hole fit condition is 2.5% interference fit, the joint with 2 kN clamping force has the highest load capacity among the joints with different clamping forces. However, when the bolt-hole fit condition is 1% interference fit, the joint with 4 kN clamping force has the highest load capacity among the joints with different clamping forces. It also can be said that the load capacity of the joints with a specific bolt-hole fit condition increases with the increase in the clamping force when the degree of the bolt-hole interference fit is lower than a certain value; however, the load capacity of the joints with a specific bolt-hole fit condition decreases with the increase in the clamping force when the degree of the bolt-hole interference fit is larger than a certain value. Similarly, the load capacity of the joints with a specific clamping force increases with the increase in the bolt-hole interference fit values when the clamping force is lower than a certain value; however, the load capacity of the joints with a specific clamping force decreases with the increase in the bolt-hole interference fit values when the clamping force is lower than a certain value. Therefore, the effects of interference fit condition and clamping force will impact each other, and the optimized interference fit value for a joint with a specified preload will not be the optimized value anymore for the joints with different preload values, and vice versa.

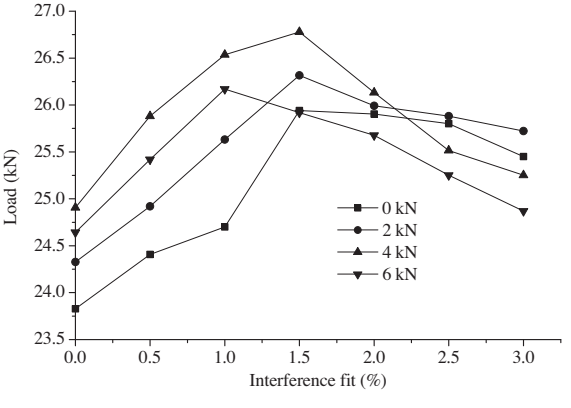

Figure 12. The combined effect of the bolt-hole fit condition and clamping force.

The assembly parameters should be taken into account together and synthetically in practical applications when the joint structures are being optimized.

7. Conclusions

In this paper, a three-dimensional finite element method is proposed and utilized to study the effects of the bolt-hole fit condition and clamping force on load capacity of a specified composite-titanium single-lap two-bolt joint. Through analysis of the simulation results, it can be concluded that:

(1) The effects of both the bolt-hole interference fit and the fastener's clamping force on the load capacities of the joints change from positive mode into negative mode with the increase in their values, and there are optimized values of them for specified joints.
(2) Too large interference fit values or clamping forces will produce premature failure around the fastener hole, and then, the load capacities of the joints will decrease.
(3) The interference fit condition and clamping force will influence each other, and they need to be taken into account synthetically during the joints being optimized.

References

[1] Xiao Y, Ishikawa T. Bearing failure in bolted composite joints: analytical tools Development. Adv. Compos. Mater. 2003;11:375–391.
[2] Olmedo A, Santiuste C. On the prediction of bolted single-lap composite joints. Compos. Struct. 2012;94:2110–2117.
[3] Kapti S, Sayman O, Ozen M, Benli Semih. Experimental and numerical failure analysis of carbon/epoxy laminated composite joints under different conditions. Mater. Des. 2010;31:3942–4933.
[4] Stickler PB, Ramulu M. Experimental study of composite T-joints under tensile and shear loading. Adv. Compos. Mater. 2006;15:193–210.
[5] Sen F, Pakdil M, Sayman O, Benli S. Experimental failure analysis of mechanically fastened joints with clearance in composite laminates under preload. Mater. Des. 2008;29:1159–1169.
[6] Cao Z, Cardew-Hall M. Interference-fit riveting technique in fibre composite laminates. Aerosp. Sci. Technol. 2006;10:327–330.
[7] Tong L. Bearing failure of composite bolted joints with non-uniform bolt-to-washer clearance. Compos. Part A-APPL. S. 2000;31:609–615.
[8] Chakherlou TN, Abazadeh B, Vogwell J. The effect of clamping compressive stresses on the fatigue life of Al 7075–T6 bolted plates at different temperatures. Eng. Fail. Anal. 2009;16:242–253.
[9] Shkarayev S. Theoretical modeling of crack arrest by inserting interference fit fasteners. Int. J. Fatigue. 2003;25:317–324.
[10] Sun HT, Van Y, Chang FK. Lateral constraining effect on bolted composite joints. In: 38th Struct. Struct. Dyn. Mater. Conf. Washington (DC): AIAA; 1997. p. 2010–2020.
[11] Yan Y, Wen WD, Chang FK, Shyprykevich P. Experimental study on clamping effects on the tensile strength of composite plates with a bolt-filled hole. Compo. Part A-APPL. S. 1999;30:1215–1229.
[12] Khashaba UA, Sallam HEM, Al-Shorbagy AE, Seif MA. Effect of washer size and tightening torque on the performance of bolted joints in composite structures. Compos. Struct. 2006;73:310–317.
[13] Rosales-Iriarte F, Fellows NA, Durodola JF. Experimental evaluation of the effect of clamping force and hole clearance on carbon composites subjected to bearing versus bypass loading. Compos. Struct. 2011;93:1096–1102.

[14] Park HJ. Effects of stacking sequence and clamping force on the bearing strengths of mechanically fastened joints in composite laminates. Compos. Struct. 2001;53:213–221.
[15] Santiuste C, Barbero E, Miguelez MH. Computational analysis of temperature effect in composite bolted joints for aeronautical applications. J. Reinf. Plast. Compos. 2011;30:3–11.
[16] Chakherlou TN, Abazadeh B. Estimation of fatigue life for plates including pre-treated fastener holes using different multiaxial fatigue criteria. Int. J. Fatigue. 2011;33:343–353.
[17] Chakherlou TN, Mirzajanzadeh M, Abazadeh B, Saeedi K. Estimation of fatigue life for plates including pre-treated fastener holes using different multiaxial fatigue criteria. Int. J. Fatigue. 2011;33:343–353.
[18] Chakherlou TN, Abazadeh B. Investigating clamping force variations in Al2024-T3 interference fitted bolted joints under static and cyclic loading. Mater. Des. 2012;37:128–136.
[19] Bunin BL. Critical composite joint subcomponents: analysis and test. Technical report No. 3711. Washington (DC): National Aeronautics and Space Administration; 1983.
[20] Kiral BG. Effect of the clearance and interference-fit on failure of the pin-loaded composites. Mater. Des. 2010;31:85–93.
[21] Kim SY, Hennigan DJ, Kim D, Seok CS. Fatigue enhancement by interference-fit in a pin-loaded glass fibre-reinforced plastics laminate. P. I. Mech. Eng. C-J. Mec. 2012;226:1437–1446.
[22] Zhao Q, Yu L, Liu H, Liu F, Ren C. The interference-fit bolted joining of hybrid metal/composite. SAE SAE Int. J. Mater. Manuf. 2013;6:19–23.
[23] Wang FL, Zhang X, Ma J, Qin W. Fatigue strength assessment of an interference fit of single-bolt, double shear lap composite bolted joints. Gongcheng Lixue/Eng. Mech. 2012;29:324–329.
[24] Wei J, Jia P, Jiao Q. An experimental study on ultimate bearing strength of composite bolt joint with interference-fit. Dev. App. Mat. 2011;26:66–69.
[25] Ran W. Study on the load capacity of composite-to-titanium bolted joints and the influence of bolt-hole fit conditions [dissertation]. Shanghai: Shanghai Jiao Tong University; 2012.
[26] HST10, HI-LITE® ST™ Pin Protruding tension head titanium, 2008 Hi-Shear corporation technical data sheet.
[27] HST1094, HI-LITE® ST™ Collar for used on HI-LITE pins, 2008 Hi-Shear corporation technical data sheet.
[28] Military handbook—MIL-HDBK-5F: metallic materials and elements for aerospace vehicle structures. U.S. Department of Defense; 2003.
[29] Huang J, Wang X. Study on tightening moment test of joint bolt in sandwich of composites. Aircr. Des. 2009;29:32–401.
[30] Mechanical Properties of CYCOM® 977–2-35%-12KHTS-134. Technical Service Cytec Engineered Materials.
[31] Mechanical Properties of CYCOM® 977–2A-37%-3KHTA-5H-280. Technical Service Cytec Engineered Materials.
[32] Mukundan S. Structural design and analysis of a lightweight composite sandwich space radiator panel [master thesis]. Texas: Mechanical Engineering, A&M University; 2003.
[33] ABAQUS documentation, version 6.9.
[34] Mohan K. Frictional analysis of aerospace alloys [dissertation]. New South Wales: University of New South Wales; 2011.
[35] Ng SP, Tse PC, Lau KJ. Progressive failure analysis of 2/2 twill weave fabric composites with moulded-in circular hole. Compos. Part-B. 2001;32:139–152.
[36] Hashin Z. Failure criteria for unidirectional fibre composite. J. Appl. Mech. 1980;47:329–334.
[37] Ye L. Role of matrix resin in delamination onset and growth in composite laminates. Compos. Sci. Technol. 1988;33:257–277.
[38] Tan SC. A progressive failure model for composite laminates containing openings. J. Compos. Mater. 1991;25:556–577.
[39] Zhao LG, Warrior NA, Long AC. Finite element modelling of damage progression in non-crimp fabric reinforced composites. Compos. Sci. Technol. 2006;66:36–50.
[40] D5961/D5961M-08,. Standard test method for bearing response of polymer matrix composite laminates. Composite materials. West Conshohocken: ASTM International; 2010.
[41] D7248/D7248M-08. Standard test method for bearing/bypass interaction response of polymer matrix composite laminates using 2-fastener specimens. Composite materials. West Conshohocken: ASTM International; 2010.

[42] ASTM D 3039/D 3039M-08. Standard test method for tensile properties of polymer matrix composite materials. West Conshohocken (PA); 2008.
[43] Ramamurthy TS. Analysis of interference fit pin joints subjected to bearing bypass loads. AIAA J. 1990;28:1800–1805.